AGU PUBLICATIONS

Geophysical Research Letters

RESEARCH LETTER
10.1002/2016GL070027

Key Points:
- We determine elasticity of single-crystal Shy-B at simultaneous high P-T conditions
- The anisotropy of Shy-B is small and cannot be the major cause for the observed seismic anisotropy in the slab regions
- Shy-B has lower velocities than those of the topmost lower mantle and could explain the observed low-velocity layer in the region

Supporting Information:
- Supporting Information S1

Correspondence to:
Z. Mao,
zhumao@ustc.edu.cn

Citation:
Li, X., Z. Mao, N. Sun, Y. Liao, S. Zhai, Y. Wang, H. Ni, J. Wang, S. N. Tkachev, and J.-F. Lin (2016), Elasticity of single-crystal superhydrous phase B at simultaneous high pressure-temperature conditions, *Geophys. Res. Lett.*, *43*, doi:10.1002/2016GL070027.

Received 13 JUN 2016
Accepted 3 AUG 2016
Accepted article online 8 AUG 2016

Elasticity of single-crystal superhydrous phase B at simultaneous high pressure-temperature conditions

HPSTAR 204-2016

Xinyang Li[1], Zhu Mao[1,2], Ningyu Sun[1], Yifan Liao[1], Shuangmeng Zhai[3], Yi Wang[1,2], Huaiwei Ni[4], Jingyun Wang[1,2], Sergey N. Tkachev[5], and Jung-Fu Lin[6]

[1]Laboratory of Seismology and Physics of Earth's Interior, School of Earth and Space Sciences, University of Science and Technology of China, Hefei, China, [2]National Geophysics Observatory, Bozhou, China, [3]Key Laboratory of High-Temperature and High-Pressure Study of the Earth's Interior, Institute of Geochemistry, Chinese Academy of Sciences, Guiyang, China, [4]CAS Key Laboratory of Crust-Mantle Materials and Environments, School of Earth and Space Sciences, University of Science and Technology of China, Hefei, China, [5]Center for Advanced Radiation Sources, University of Chicago, Chicago, Illinois, USA, [6]Department of Geological Sciences, Jackson School of Geosciences, The University of Texas at Austin, Austin, Texas, USA

Abstract We investigated the combined effect of pressure and temperature on the elasticity of single-crystal superhydrous phase B (Shy-B) using Brillouin scattering and X-ray diffraction up to 12 GPa and 700 K. Using the obtained elasticity, we modeled the anisotropy of Shy-B along slab geotherms, showing that Shy-B has a low anisotropy and cannot be the major cause of the observed anisotropy in the region. Modeled velocities of Shy-B show that Shy-B will be shown as positive velocity anomalies at the bottom transition zone. Once Shy-B is transported to the topmost lower mantle, it will exhibit a seismic signature of lower velocities than topmost lower mantle. We speculate that an accumulation of hydrous phases, such as Shy-B, at the topmost lower mantle with a weight percentage of ~17–26% in the peridotite layer as subduction progresses could help explain the observed 2–3% low shear velocity anomalies in the region.

1. Introduction

Water can be delivered to the Earth's mantle through sinking subduction slabs carrying a number of hydrous minerals in the layers of mantle lithosphere and oceanic crust [*Hacker et al*., 2003; *Ohtani*, 2005; *Peacock*, 1990; *Stern*, 2002]. The discovery of a diamond with a hydrous ringwoodite inclusion containing as much as 1.5 wt % water has revealed that some regions of the Earth's transition zone could be highly hydrated [*Pearson et al*., 2014; *Thomas et al*., 2015]. Meanwhile, recent seismological studies have presented evidence of low-velocity layers at the topmost lower mantle, which have also been interpreted to be caused by the presence of melting associated with dehydration reactions [*Liu et al*., 2016; *Schmandt et al*., 2014]. All of these findings indicate that some hydrous minerals can survive the dehydration process in the subduction zone and be transported to depths at the bottom transition zone and the topmost lower mantle through sinking subduction slabs [*Liu et al*., 2016; *Pearson et al*., 2014; *Schmandt et al*., 2014].

Since most hydrous minerals in the subduction slabs, such as antigorite, lawsonite, and amphibole, decompose and release water to the overlying mantle wedge at depths less than 300 km, dense hydrous magnesium silicates (DHMSs), particularly superhydrous phase B (Shy-B), have been proposed to be one of the major phases to transport water to the bottom transition zone and the topmost lower mantle [e.g., *Fumagalli and Poli*, 2005; *Ohtani*, 2005; *Schmidt*, 1995; *Shieh et al*., 2000; *Ulmer and Trommsdorff*, 1995]. Shy-B with an ideal chemical formula of $Mg_{10}Si_3H_4O_{18}$ containing 5.8 wt % water can be formed by a mantle assemblage with a Mg/Si ratio of 1.5–2.0 below 1200°C and is stable up to 30 GPa and 1400°C [*Gasparik*, 1993; *Komabayashi*, 2006; *Ohtani et al*., 1995; *Ohtani et al*., 2003; *Pacalo and Parise*, 1992; *Shieh et al*., 2000]. Although the maximum amount of Shy-B in the peridotite slab layer was estimated to be 22–31 wt % based on a mass balance calculation from the partitioning of water between hydrous mantle minerals, the abundance of Shy-B in the slabs is highly uncertain [*Ohtani et al*., 2004; *Ohtani*, 2005]. Identifying the presence of Shy-B remains to be a key subject for understanding water transportation and the cause of the observed low-velocity layers in the topmost lower mantle.

Comparing the velocity-density profiles of Shy-B modeled using its elasticity at high pressure-temperature (P-T) with the seismic images of the mantle is of particular importance because it can help decipher the presence of Shy-B in the mantle transition zone and topmost lower mantle. High P-T X-ray diffraction

(XRD) has been applied to investigate the equation of state (EoS) parameters of Shy-B up to 27 GPa and 1400°C [*Crichton et al*., 1999; *Inoue et al*., 2006; *Kudoh et al*., 1994; *Litasov et al*., 2007]. At ambient conditions, the obtained isothermal bulk modulus, K_{T0}, ranges from 132 to 145 GPa, much lower than that of transition zone majorite and ringwoodite and lower mantle ferropericlase, bridgmanite, and $CaSiO_3$-perovskite [*Crichton et al*., 1999; *Inoue et al*., 2006; *Irifune et al*., 2008; *Jacobsen et al*., 2002; *Kudoh et al*., 1994; *Mao et al*., 2015; *Sinogeikin et al*., 1998]. It should be noted that K_{T0} cannot be independently constrained by the XRD measurements because of the well-known trade-off between K_{T0} and its pressure derivative, K_{T0}'. Elasticity of single-crystal Shy-B has been investigated by Brillouin spectroscopy up to 17 GPa and 300 K, which yields crucial constraints on the shear modulus and the anisotropy of Shy-B [*Pacalo and Weidner*, 1996; *Rosa et al*., 2015]. The adiabatic bulk modulus, K_{S0}, at ambient conditions has been determined to be 150–154 GPa with its pressure derivative, $K_{S0}' = 4.7(2)$, while the shear modulus, G_0, is 97–99 GPa with $G_0' = 1.44(5)$ [*Pacalo and Weidner*, 1996; *Rosa et al*., 2015]. Compared to the experimental results, a theoretical study predicted a higher K_{S0} of 161.8(0.1) GPa with $K_{S0}' = 4.4(0.1)$ and $G_0 = 102.5$ GPa with $G_0' = 1.6$ [*Mookherjee and Tsuchiya*, 2015]. Most importantly, the combined effect of pressure and temperature on the elasticity of Shy-B is unknown. The elasticity of Shy-B at high P-T is needed to reliably model its velocity profiles in the transition zone and topmost lower mantle in order to reveal the role of the presence of Shy-B on seismic signatures in the region.

In this work, we have performed high P-T Brillouin scattering and single-crystal XRD measurements to determine the elasticity of single-crystal Shy-B up to 12 GPa and 700 K in an externally heated diamond anvil cell (EHDAC) [*Kantor et al*., 2012]. Using the obtained elasticity, we have modeled the anisotropy and velocity of Shy-B at P-T conditions relevant to the subduction slabs to examine its seismic signatures. Comparing the modeled results of Shy-B to the velocity profiles of the normal mantle provides new insight in our understanding of the potential water-rich region in the mantle, including the observed low-velocity layers at the topmost lower mantle.

2. Experiments

Single crystals of Shy-B were synthesized at 20 GPa and 1573 K for 20 h from a mixture of MgO (52.06 wt %), SiO_2 (29.1 wt %), and $Mg(OH)_2$ (18.83 wt %) powders by using the USSA-5000 ton Kawai-type apparatus installed at the Institute for Study of Earth's Interior, Okayama University. We performed single-crystal X-ray diffraction (XRD) at ambient conditions to confirm that the obtained crystals were in Shy-B structure with *Pnnm* space group. The lattice parameters of Shy-B samples at ambient conditions are $a = 14.028(6)$ Å, $b = 5.103(1)$ Å, and $c = 8.719(1)$ Å. The obtained single crystals were also examined by the electron microprobe at Key Laboratory of Crust-Mantle Materials and Environments, University of Science and Technology of China, showing a composition of 28.06 wt % SiO_2 and 62.92 wt % MgO. The water content of 9.0 wt % for the synthesized Shy-B was calculated using the weight deficiency in the sum of all oxides, yielding a composition of $Mg_{9.38}Si_{2.81}H_{6.01}O_{18}$ with a density of 3.197(5) g/cm^3.

We selected two pieces of Shy-B single crystals that possessed nearly orthogonal crystallographic orientation. The crystallographic planes of the two pieces are (0.91, 0.28, 0.30) and (−0.20, 0.60, 0.80), as determined by single-crystal XRD at beamline sector 13-BMD of the Advanced Photon Source (APS). We double-side polished both sample pieces to thin platelets ~30 μm in thickness. Re was used as the gasket material with a 300 μm hole drilled at the center of the indentation. We selected one platelet from each orientation and loaded it into the sample chamber of the EHDAC. A ruby sphere and Pt foil of ~10 μm were loaded next to the sample platelets. Ne was used as the pressure medium, while the Pt foil was used as the pressure calibrant during the high P-T measurements. Heating at high pressures was achieved by supplying electricity to a cylindrical alumina ceramic heater equipped in the EHDAC. The alumina heater was coiled by Pt wires 200 μm in diameter. An R-type thermocouple used as the temperature calibrant was glued ~500 μm away from one of the diamond anvils. The uncertainty of the temperature measurements is less than ±5 K.

Brillouin spectroscopy was performed at beamline sector 13-BMD of APS up to 12 GPa and at 300 K, 500 K, and 700 K, in a symmetric forward scattering geometry [*Sinogeikin et al*., 2006]. With measured Brillouin frequency shift, $\Delta\upsilon_B$, the acoustic velocities, v, can be calculated as follows:

$$v = \frac{\Delta\upsilon_B \lambda_0}{2\sin(\theta/2)} \quad (1)$$

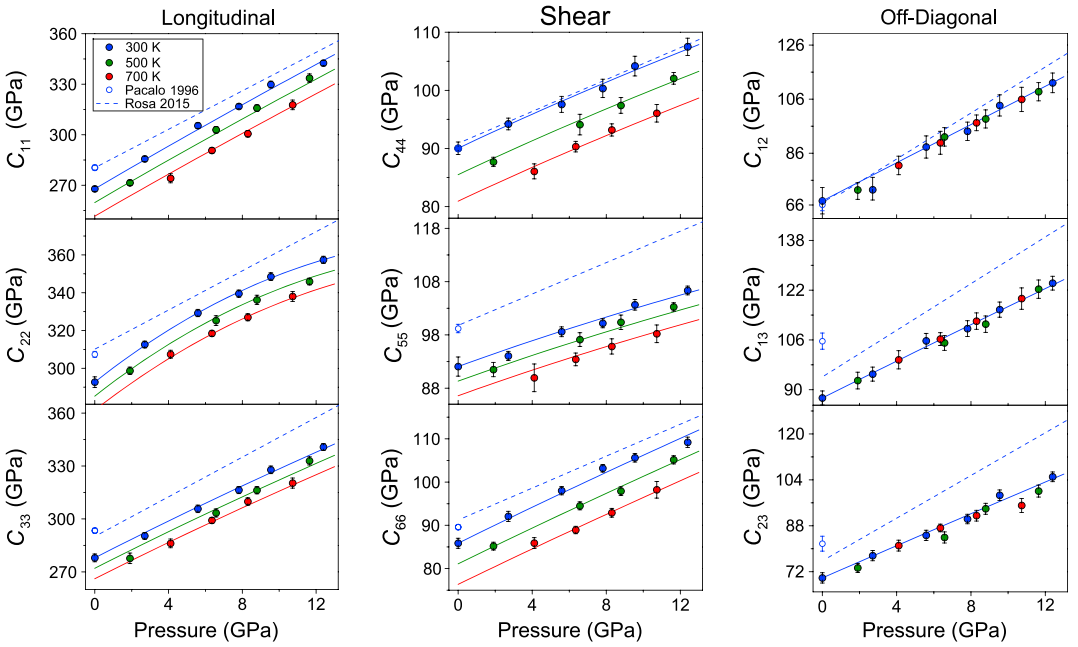

Figure 1. High P-T elasticity of single-crystal Shy-B. Blue, green, and red solid circles: this study at 300 K, 500 K, and 700 K, respectively; open circles: results at ambient conditions from *Pacalo and Weidner* [1996]; solid lines: fitting results using the third-order finite strain theory; dashed lines: results at 300 K from *Rosa et al.* [2015].

where θ is 50° of the external scattering angle, and λ_0 is the laser wavelength of 532 nm. The density of the Shy-B sample at each P-T condition after the Brillouin measurements was determined by the single-crystal XRD.

3. Results

Shy-B in the orthorhombic setting can be characterized by nine independent elastic constants. Following the Christoffel's equation, we simultaneously fitted the velocity of two platelets obtained at various azimuthal angles over a range of 180°, which yields crucial constraints on nine elastic constants [*Every*, 1980]:

$$\left|c_{ijkl}n_j n_l - \rho v^2 \delta_{ik}\right| = 0 \tag{2}$$

where n_j and n_l are the direction cosines of the phonon along the propagation direction, ρ is the density at each P-T condition, and δ_{ik} is the Kronecker delta function. C_{ijkl} is the elastic constant in full suffix notation, but we used the reduced notation, C_{ij}, in our study.

At a given temperature, all but one elastic constant increases linearly with pressure, whereas the longitudinal modulus, C_{22}, shows a slight downward curvature (Figure 1). Although increasing temperature offsets all of the longitudinal and shear moduli to a lower value at a given pressure, elevated temperature has a negligible effect on the off-diagonal moduli (C_{12}, C_{23}, and C_{13}) after considering experimental errors. With the obtained C_{ij}s (Table S1 in the supporting information), we calculated the adiabatic bulk and shear moduli (K_S and G) at each experimental P-T condition using the Voigt-Reuss-Hill average. The adiabatic bulk and shear moduli at ambient conditions (K_{S0} and G_0) are 143(1) and 94(1) GPa, respectively.

Combining the Brillouin and XRD measurements allows us to establish an equation of state (EoS) for Shy-B, which is independent of any pressure scale (supporting information) [*Li et al.*, 2006a; *Zha et al.*, 2000]. Using the literature thermal expansion coefficient, $\alpha = 3.6 \times 10^{-5}\,\mathrm{K}^{-1}$, and Grüneisen parameter, $\gamma = 1.8$ [*Komabayashi and Omori*, 2006; *Inoue et al.*, 2006; *Litasov et al.*, 2007; *Rosa et al.*, 2015], we convert K_S of Shy-B at 300 K into the isothermal bulk modulus, K_T, following (Table S2):

$$K_T = K_S/(1 + \alpha\gamma T) \tag{3}$$

Fitting the K_T–ρ data sets at 300 K using the third-order finite-strain equations allows us to constrain the pressure derivative of the bulk modulus, $K_{T0}' = 4.0(1)$. With known K_{T0}, K_T', and ρ, we determined the primary P-ρ-T

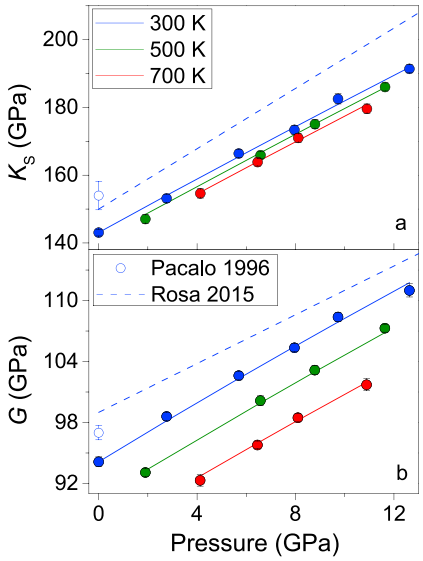

Figure 2. High P-T bulk and shear moduli of Shy-B. Blue, green, and red solid circles: this study at 300 K, 500 K, and 700 K, respectively; open circles: results at ambient conditions from *Pacalo and Weidner* [1996]; solid lines: fitting results using the third-order finite strain theory; dashed lines: results at 300 K from *Rosa et al.* [2015].

EoS of Shy-B with a $(\partial K_T/\partial T)_P$ value of −0.021(1) GPa/K and $(\partial K_S/\partial T)_P = -0.012(1)$ GPa/K [*Speziale and Duffy*, 2002], and then calculated the absolute values of pressures at each experimental conditions, which are independent of any pressure scales (Table S1). We note that the difference in pressure computed using the primary *P-ρ-T* EoS of Shy-B and that from Pt placed next to the Shy-B sample is up to 0.3 GPa at 10.7 GPa and 700 K. For each individual C_{ij} and the shear moduli, their pressure and temperature derivative were determined by fitting the elastic moduli at high P-T using the third/fourth-order finite strain EoS (Figures 1 and 2 and Table S2).

4. Discussion

Combining Brillouin spectroscopy and single-crystal XRD measurements, we have determined the elasticity of Shy-B at simultaneous high P-T conditions. Compared to previous experimental results [*Pacalo and Weidner*, 1996], the obtained C_{ij}s, aggregate K_S, and G at ambient conditions, with the exception of C_{44} and C_{12}, are 3–17% lower, potentially due to the higher water content of our synthesized Shy-B single crystals. The shear modulus, C_{44}, and longitudinal modulus, C_{12}, are not sensitive to the variation of the water content. The Shy-B samples used in this study contain 9.0 wt % water with a composition of $Mg_{9.38}Si_{2.81}H_{6.01}O_{18}$, which is greater than the water content of 5.8 wt % in an ideal formula of $Mg_{10}Si_3H_4O_{18}$. Although composition of our starting material corresponds to an ideal formula of Shy-B ($Mg_{10}Si_3H_4O_{18}$), the synthesized Shy-B single crystals have a higher concentration of Mg and Si defects. In this case, our Shy-B could accommodate a greater amount of water than the corresponding phase with the ideal formula of 5.8 wt % water and thus has a lower elastic moduli than found in previous studies [*Pacalo and Weidner*, 1996].

In addition, a recent Brillouin study on the elasticity of Shy-B reported that C_{ij}s, aggregate K_S, and G at high pressures and 300 K are greater than our values [*Rosa et al.*, 2015]. We note that the water content in *Rosa et al.* [2015], calculated from the deficiency of the total sum of oxides, should be 7.54 wt %, which is inconsistent with the value of 3.85 wt % from their reported chemical formula. The chemical formula of Shy-B in *Rosa et al.* [2015] is thus problematic. We revaluated the elasticity of Shy-B in *Rosa et al.* [2015] with a correct density of 3.240(4) g/cm^3. Together with the XRD results, we note that the elasticity of Shy-B exhibits a linear reduction with increasing water content (Figure S2 in the supporting information). We further compared the experimental results to the theoretical prediction (Figure S3) [*Mookherjee and Tsuchiya*, 2015]. The pressure dependence of most elastic moduli from theoretical predictions is similar to the experimental results, although their absolute values are greater (Figure S3 and S4) [*Mookherjee and Tsuchiya*, 2015].

Using the obtained elasticity at high P-T, we calculated the maximum azimuthal V_P anisotropy [$A_P = (V_{P,\max} - V_{P,\min})/V_{P,\text{avg}}$] and V_S splitting [$A_S^{PO} = (V_{S2} - V_{S1})/V_{S,\text{avg}}$] of Shy-B along hot and cold slab geotherms, respectively, and compared them with the anisotropy of major mantle minerals calculated using literature results (Figure 3). Here the temperature of the hot slabs is 400°C lower than the mantle 1400°C adiabat, while the temperature of the cold slabs is 800°C lower [*Komabayashi et al.*, 2002; *Litasov and Ohtani*, 2003; *Thompson*, 1992]. Both A_P and A_S^{PO} of mantle minerals, including anhydrous and hydrous ringwoodite, bridgmanite, ferropericlase, and $CaSiO_3$-perovskite, were calculated along a 1400°C adiabat [*Jacobsen et al.*, 2002; *Jackson et al.*, 2006; *Kawai and Tsuchiya*, 2015; *Mao et al.*, 2012; *Sinogeikin et al.*, 2003; *Shukla et al.*, 2015]. Since we lack constraints on the effect of temperature on the elasticity of single-crystal majorite, and majorite is nearly elastically isotropic at high pressures and 300 K [*Murakami et al.*, 2008], the anisotropy of majorite is

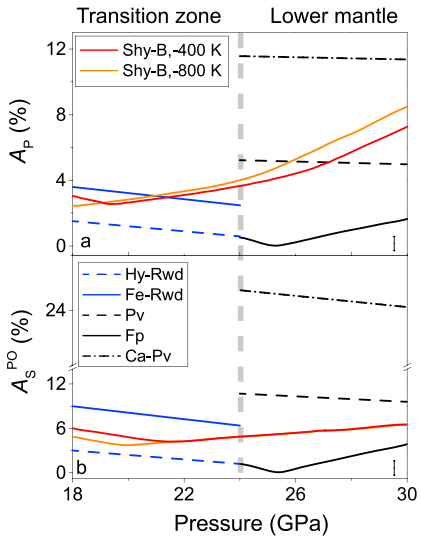

Figure 3. Maximum azimuthal (a) V_P anisotropy (A_P) and (b) V_S splitting (A_S^{PO}) of Shy-B along slab geotherms and mantle minerals along 1400°C adiabat. Red lines: Shy-B along hot slab geotherm, which is 400 K colder than the 1400°C adiabat [*Brown and Shankland*, 1981]; orange lines: Shy-B along cold slab geotherm, which is 800 K colder than the 1400°C adiabat [*Brown and Shankland*, 1981]; blue line: Fe-Rwd, dry ringwoodite [*Nishihara et al*., 2004; *Sinogeikin et al*., 1998; *Sinogeikin et al*., 2003; *Watanabe*, 1987]; blue dashed line: Hy-Rwd, ringwoodite with 1 wt % water [*Mao et al*., 2012; *Nishihara et al*., 2004; *Watanabe*, 1987]; black dashed line: Pv, bridgmanite [*Anderson et al*., 1995; *Murakami et al*., 2007; *Murakami et al*., 2012; *Shukla et al*., 2015; *Sinogeikin et al*., 2004; *Wang et al*., 1994]; black dash-dotted line: Ca-Pv, $CaSiO_3$-perovsite [*Kawai and Tsuchiya*, 2015; *Li et al*., 2006b]; black line: Fp with 17 mol % Fe, ferropericlase [*Isaak et al*., 1989; *Jackson et al*., 2006; *Jacobsen et al*., 2002; *Mao et al*., 2011; *Murakami et al*., 2012; *Suzuki*, 1975].

not considered here. $CaSiO_3$-perovskite exhibits a pretty high anisotropy due to a small shear modulus suggested by a recent theoretical study [*Kawai and Tsuchiya*, 2015].

Our modeling shows that both A_P and A_S^{PO} of Shy-B display a weak dependence on temperature from the bottom transition zone to the topmost lower mantle (Figure 3). Along both hot and cold slab geotherms, A_P and A_S^{PO} of Shy-B are comparable to those of anhydrous ringwoodite but slightly greater than that of ringwoodite with 1 wt % water. Although increasing pressure (depth) from 24 GPa to 30 GPa leads to an increase in A_P of Shy-B from 4% to 8%, A_P of Shy-B is still much smaller than that of $CaSiO_3$-perovskite, and is comparable to that of bridgmanite, but greater than ferropericlase. A_S^{PO} of Shy-B is smaller than that of $CaSiO_3$-perovskite and bridgmanite and only slightly greater than that of ferropericlase. Due to the small value of A_P and A_S^{PO}, Shy-B cannot be the major cause for the observed seismic anisotropy at the bottom transition zone and the topmost lower mantle [e.g., *Chen and Brudzinski*, 2003; *Long*, 2013; *Mookherjee and Tsuchiya*, 2015; *Rosa et al*., 2015].

5. Geophysical Implications

Recent seismic studies using different methods have identified the existence of a low-velocity layer at depths of the topmost lower mantle near the subduction slabs [*Liu et al*., 2016; *Schmandt et al*., 2014; *Tang et al*., 2014]. The observed low-velocity layer has been explained either as a result of dehydration melting [*Liu et al*., 2016; *Schmandt et al*., 2014] or decompression melting due to the mantle upwelling [*Tang et al*., 2014]. Since Shy-B is expected to be one of the carriers of water to the bottom transition zone and topmost lower mantle, comparing the modeled velocity of Shy-B to seismic images is of particular importance in understanding the cause for the observed low-velocity layers.

Here we have modeled V_P and V_S of Shy-B along both hot and cold slab geotherms using the obtained elasticity (Figure 4) [*Komabayashi et al*., 2002; *Litasov and Ohtani*, 2003; *Thompson*, 1992]. Although modeling the velocity of Shy-B requires extrapolating our experimental data to the relevant pressure and temperature conditions of the mantle, our modeling provides a first-order estimation on how the presence of Shy-B may influence the velocity structure at the bottom of the transition zone and the topmost lower mantle. For the normal mantle, we assumed that it is in a pyrolitic composition along a 1400°C adiabat. V_P and V_S of a pyrolitic mantle were modeled at both dry and hydrous conditions using the elasticity and density data in literature (Table S4). In our hydrous model, we consider the effect of water on V_P and V_S of a pyrolitic mantle in terms of its effect on the velocity of ringwoodite because the experimental constraints on the elasticity of majorite are not available. The water content in ringwoodite is 1 wt %, which is close to the maximum amount of water that could be stored in ringwoodite at the bottom of the transition zone [*Inoue et al*., 2010; *Kohlstedt et al*., 1996; *Litasov and Ohtani*, 2003; *Pacalo and Weidner*, 1996]. The lower mantle was assumed to be dry because the water storage capacity of lower mantle minerals was previously reported to be significantly lower than that of minerals in the subduction slabs and the transition zone [*Bolfan-Casanova*, 2005; *Hernandez et al*., 2013; *Inoue et al*., 2010; *Litasov and Ohtani*, 2003; *Murakami et al*., 2002; *Ohtani*, 2005; *Palus*, 2015].

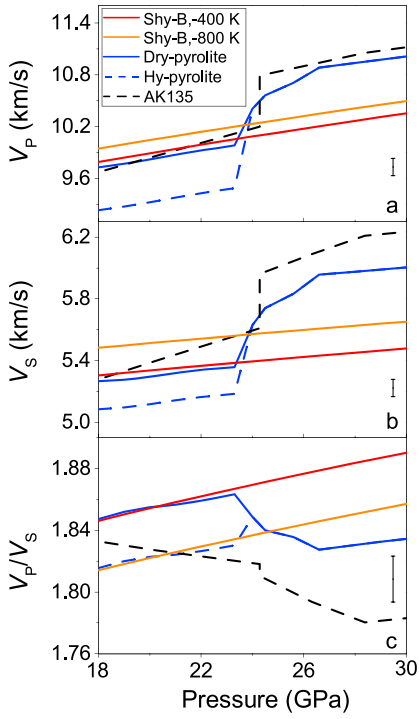

Figure 4. Longitudinal (V_P) and shear wave (V_S) velocities and V_P/V_S of Shy-B along slab geotherms compared with those of a pyrolitic mantle. Red lines: Shy-B along hot slab geotherm, which is 400 K colder than the 1400°C adiabat [*Brown and Shankland*, 1981]; orange lines: Shy-B along cold slab geotherm, which is 800 K colder than the 1400°C adiabat [*Brown and Shankland*, 1981]; blue lines: dry pyrolitic mantle along 1400°C adiabat; blue dashed lines: hydrous pyrolitic mantle along 1400°C adiabat; black dashed lines: AK135 [*Kennett et al.*, 1995].

At depths near the bottom transition zone, our modeling results show that Shy-B along a hot slab geotherm has similar V_P, V_S, and V_P/V_S as those of a dry pyrolitic mantle, indicating that no amount of Shy-B in the slab would be detectible (Figure 4). Along a cold slab geotherm, Shy-B has a V_P and V_S 2.3(3)% and 4.2(4)% greater than that of the dry mantle, respectively, but has a slightly lower V_P/V_S ratio. The difference in V_P/V_S ratio between Shy-B and the dry pyrolitic mantle could be negligible considering the errors in our modeling. If the peridotite layer of some cold slabs contains a maximum possible water storage capacity with 22 wt % Shy-B [*Ohtani et al.*, 2004; *Ohtani*, 2005], the presence of this amount of Shy-B will produce a 0.6–1.0(4)% positive velocity anomaly. We then considered a hydrous mantle transition zone with 1 wt % water in ringwoodite, which has a V_P and V_S 5.0(5)% and 3.4(4)% lower than those of a dry pyrolitic mantle, respectively (Figure 4). Along a hot slab geotherm, V_P and V_S of Shy-B is ~4.3–6.0(5)% greater than that of a hydrous mantle, while the difference in V_P and V_S between Shy-B along the cold slab geotherm and the hydrous transition zone is up to ~7.6(5)%. The presence of 22–31 wt % Shy-B in a water-saturated peridotite layer along a hot or cold slab geotherm would produce an ~1.0–2.7(4)% positive velocity anomaly using the velocity of the hydrous transition zone as the reference [*Ohtani et al.*, 2004; *Ohtani*, 2005]. As a result, Shy-B in the slabs would be either seismically invisible in hot regions or shown as positive velocity anomalies in cold regions at depths of the bottom of the transition zone.

As the subduction continues, Shy-B could be transported to the topmost lower mantle. Since the water storage capacity of lower mantle minerals is significantly lower than that of minerals in transition zone and slabs, we have assumed a dry lower mantle. Along both hot and cold slab geotherms, Shy-B has a V_P and V_S 5–10% lower than the topmost lower mantle, whereas its V_P/V_S ratio is slightly greater (Figure 4). Considering its low density compared to lower mantle minerals, Shy-B may accumulate at depths of the topmost lower mantle as long as the subduction continues. We estimated that an accumulation of Shy-B with a weight percentage of 17–26% in the peridotite layer of the slabs at the topmost lower mantle can produce an ~2–3% low shear velocity anomaly, which can help explain the observed low-velocity layers in some regions of the lower mantle below the depressed 660–km discontinuity [*Liu et al.*, 2016; *Schmandt et al.*, 2014; *Tang et al.*, 2014].

It should be noted that the modeling above only calculated the velocities for Mg end-member of Shy-B. Shy-B in the slabs may contain a certain amount of Fe. The presence of Fe can increase the density of Shy-B, which can help Shy-B sink to the lower mantle, and affects V_P and V_S of Shy-B. However, the velocity of Fe-bearing Shy-B cannot be modeled because the elasticity of Fe-bearing Shy-B at simultaneous high P-T conditions is not known [*Crichton et al.*, 1999]. Meanwhile, phase D is another important water-bearing phase at the bottom transition zone and the topmost lower mantle [e.g., *Ohtani*, 2005]. We do not model the velocities of phase D because the experimental constraints on the combined effect of pressure and temperature on the elasticity of phase D are not available [*Chang et al.*, 2013; *Liu et al.*, 2004; *Rosa et al.*, 2012]. Future studies are thus expected to provide more detailed information on the elasticity of Fe-bearing Shy-B and phase D, which are needed to identify the presence of hydrous phases, such as Shy-B and phase D, and understand the potential cause for the low-velocity layers at the topmost lower mantle.

Acknowledgments
Z. Mao acknowledges support from the NSFC (41590621 and 41374092). This work is also supported from the Fundamental Research Funds for the Central Universities in China (WK2080000052). The NSF Geophysics Program, Deep Carbon Observatory of the Sloan Foundation, and the Center for HPSTAR provide support for J.F. Lin. The experimental work performed at GSECARS, APS, and ANL is supported by DOE (DE-FG02-94ER14466) and the NSF (EAR-0622171). Experimental data for Figures 1 and 2 are listed in Table S1. Data for modeling Figure 4 are available in the Table S4. A more detailed discussion of the methodology can be found in the supporting information [*Birch*, 1978; *Nishihara et al*., 2005; *Zou et al*., 2012].

References

Anderson, O. L., K. Masuda, and D. G. Isaak (1995), A new thermodynamic approach for high-pressure physics, *Phys. Earth Planet. Int.*, *91*, 3–16.
Birch, F. (1978), Finite strain isotherm and velocities for single-crystal and polycrystalline NaCl at high-pressures and 300°K, *J. Geophys. Res.*, *83*, 1257–1268, doi:10.1029/JB083iB03p01257.
Bolfan-Casanova, N. (2005), Water in the Earth's mantle, *Mineral. Mag.*, *69*, 229–257.
Brown, J. M., and T. J. Shankland (1981), Thermodynamic parameters in the Earth as determined from seismic profiles, *Geophys. J. R. Astron. Soc.*, *66*, 579–596.
Chang, Y. Y., et al. (2013), Spin transition of Fe^{3+} in Al-bearing phase D: An alternative explanation for small-scale seismic scatterers in the mid-lower mantle, *Earth Planet. Sci. Lett.*, *382*, 1–9.
Chen, W. P., and M. R. Brudzinski (2003), Seismic anisotropy in the mantle transition zone beneath Fiji-Tonga, *Geophys. Res. Lett.*, *30*(13), 1682, doi:10.1029/2002GL016330.
Crichton, W. A., N. L. Ross, and T. Gasparik (1999), Equations of state of magnesium silicates anhydrous B and superhydrous B, *Phys. Chem. Miner.*, *26*, 570–575.
Every, A. G. (1980), General closed-form expressions for acoustic-waves in elastically anisotropic solids, *Phys. Rev. B*, *22*, 1746–1760.
Fumagalli, P., and S. Poli (2005), Experimentally determined phase relations in hydrous peridotites to 6.5 GPa and their consequences on the dynamics of subduction zones, *J. Petrol.*, *46*, 555–578.
Gasparik, T. (1993), The role of volatiles in the transition zone, *J. Geophys. Res.*, *98*, 4287–4299, doi:10.1029/92JB02530.
Hacker, B. R., G. A. Abers, and S. M. Peacock (2003), Subduction factory—1. Theoretical mineralogy, densities, seismic wave speeds, and H_2O contents, *J. Geophys. Res.*, *108*(B1), 2029, doi:10.1029/2001JB001127.
Hernandez, E. R., D. Alfe, and J. Brodholt (2013), The incorporation of water into lower-mantle perovskites: A first-principles study, *Earth Planet. Sci. Lett.*, *364*, 37–43.
Inoue, T., T. Ueda, Y. Higo, A. Yamada, T. Irifune, and K. I. Funakoshi (2006), High-pressure and high-temperature stability and equation of state of superhydrous phase B, in *Earth's Deep Water Cycle*, edited by S. D. Jacobsen and S. Lee, pp. 147–157, AGU, Washington, D. C.
Inoue, T., T. Wada, R. Sasaki, and H. Yurimoto (2010), Water partitioning in the Earth's mantle, *Phys. Earth Planet. Int.*, *183*, 245–251.
Irifune, T., Y. Higo, T. Inoue, Y. Kono, H. Ohfuji, and K. Funakoshi (2008), Sound velocities of majorite garnet and the composition of the mantle transition region, *Nature*, *451*, 814–817.
Isaak, D. G., O. L. Anderson, and T. Goto (1989), Measured elastic-moduli of single-crystal MgO up to 1800 K, *Phys. Chem. Miner.*, *16*, 704–713.
Jackson, J. M., S. V. Sinogeikin, S. D. Jacobsen, H. J. Reichmann, S. J. Mackwell, and J. D. Bass (2006), Single-crystal elasticity and sound velocities of $(Mg_{0.94}Fe_{0.06})O$ ferropericlase to 20 GPa, *J. Geophys. Res.*, *111*, B09203, doi:10.1029/2005JB004052.
Jacobsen, S. D., H. J. Reichmann, H. A. Spetzler, S. J. Mackwell, J. R. Smyth, R. J. Angel, and C. A. McCammon (2002), Structure and elasticity of single-crystal (Mg,Fe)O and a new method of generating shear waves for gigahertz ultrasonic interferometry, *J. Geophys. Res.*, *107*(B2), 2037, doi:10.1029/2001JB000490.
Kantor, I., V. Prakapenka, A. Kantor, P. Dera, A. Kurnosov, S. Sinogeikin, N. Dubrovinskaia, and L. Dubrovinsky (2012), BX90: A new diamond anvil cell design for X-ray diffraction and optical measurements, *Rev. Sci. Instrum.*, *83*, doi:10.1063/1.4768541.
Kawai, K., and T. Tsuchiya (2015), Small shear modulus of cubic $CaSiO_3$ perovskite, *Geophys. Res. Lett.*, *42*, 2718–2726, doi:10.1002/2015GL063446.
Kennett, B. L. N., E. R. Engdahl, and R. Buland (1995), Constraints on seismic velocities in the Earth from travel-times, *Geophys. J. Int.*, *122*, 108–124.
Kohlstedt, D. L., H. Keppler, and D. C. Rubie (1996), Solubility of water in the alpha, beta and gamma phases of $(Mg,Fe)_2SiO_4$, *Contrib. Mineral. Petr.*, *123*, 345–357.
Komabayashi, T. (2006), Phase relations of hydrous peridotite: Implications for water circulation in the Earth's mantle, in *Earth's Deep Water Cycle*, edited by S. D. Jacobsen, and S. Lee, pp. 29–43, AGU, Washington, D. C.
Komabayashi, T., and S. Omori (2006), Internally consistent thermodynamic data set for dense hydrous magnesium silicates up to 35 GPa, 1600°C: Implications for water circulation in the Earth's deep mantle, *Phys. Earth Planet. Int.*, *156*, 89–107.
Komabayashi, T., S. Omori, and S. Maruyama (2002), A new petrogenetic grid for hydrous slab peridotite down to 800 km depth, paper presented at Abst. Superplume Int. Workshop, TIT, Tokyo.
Kudoh, Y., T. Nagase, S. Ohta, S. Sasaki, M. Kanzaki, and M. Tanaka (1994), Crystal-structure and compressibility of superhydrous phase-B, $Mg_{20}Si_6H_8O_{36}$, paper presented at AIP Conf. Proc., Colorado Springs, Colo.
Li, B., K. Woody, and J. Kung (2006a), Elasticity of MgO to 11 GPa with an independent absolute pressure scale: Implications for pressure calibration, *J. Geophys. Res.*, 111, B11206, doi:10.1029/2005JB004251.
Li, L., D. J. Weidner, J. Brodholt, D. Alfe, G. D. Price, R. Caracas, and R. Wentzcovitch (2006b), Elasticity of $CaSiO_3$ perovskite at high pressure and high temperature, *Phys. Earth Planet. Int.*, *155*, 249–259.
Litasov, K., and E. Ohtani (2003), Stability of various hydrous phases in CMAS pyrolite-H_2O system up to 25 GPa, *Phys. Chem. Miner.*, *30*, 147–156.
Litasov, K. D., E. Ohtani, S. Ghosh, Y. Nishihara, A. Suzuki, and K. Funakoshi (2007), Thermal equation of state of superhydrous phase B to 27 GPa and 1373 K, *Phys. Earth Planet Int.*, *164*, 142–160.
Liu, L. G., K. Okamoto, Y. J. Yang, C. C. Chen, and C. C. Lin (2004), Elasticity of single-crystal phase D (a dense hydrous magnesium silicate) by Brillouin spectroscopy, *Solid State Commun.*, *132*, 517–520.
Liu, Z., J. Park, and S. I. Karato (2016), Seismological detection of low velocity anomalies surrounding the mantle transition zone in Japan subduction zone, *Geophys. Res. Lett.*, *43*, 2480–2487, doi:10.1002/2015GL067097.
Long, M. D. (2013), Constraints on subduction geodynamics from seismic anisotropy, *Rev. Geophys.*, *51*, 76–112, doi:10.1002/rog.20008.
Mao, Z., J. F. Lin, J. Liu, and V. B. Prakapenka (2011), Thermal equation of state of lower-mantle ferropericlase across the spin crossover, *Geophys. Res. Lett.*, *38*, L02399, doi:10.1029/2011GL049915.
Mao, Z., J. F. Lin, S. D. Jacobsen, T. S. Duffy, Y. Y. Chang, J. R. Smyth, D. J. Frost, E. H. Hauri, and V. B. Prakapenka (2012), Sound velocities of hydrous ringwoodite to 16 GPa and 673 K, *Earth Planet. Sci. Lett.*, *331*, 112–119.
Mao, Z., D. W. Fan, J. F. Lin, J. Yang, S. N. Tkachev, K. Zhuravlev, and V. B. Prakapenka (2015), Elasticity of single-crystal olivine at high pressures and temperatures, *Earth Planet. Sci. Lett.*, *426*, 204–215.
Mookherjee, M., and J. Tsuchiya (2015), Elasticity of superhydrous phase B, $Mg_{10}Si_3O_{14}(OH)_4$, *Phys. Earth Planet Int.*, *238*, 42–50.
Murakami, M., K. Hirose, H. Yurimoto, S. Nakashima, and N. Takafuji (2002), Water in Earth's lower mantle, *Science*, *295*, 1885–1887.
Murakami, M., S. V. Sinogeikin, H. Hellwig, J. D. Bass, and J. Li (2007), Sound velocity of $MgSiO_3$ perovskite to Mbar pressure, *Earth Planet. Sci. Lett.*, *256*, 47–54.

Murakami, M., S. V. Sinogeikin, K. Litasov, E. Ohtani, and J. D. Bass (2008), Single-crystal elasticity of iron-bearing majorite to 26 GPa: Implications for seismic velocity structure of the mantle transition zone, *Earth Planet. Sci. Lett.*, *274*, 339–345.
Murakami, M., Y. Ohishi, N. Hirao, and K. Hirose (2012), A perovskitic lower mantle inferred from high-pressure, high-temperature sound velocity data, *Nature*, *485*, 90–U118.
Nishihara, Y., E. Takahashi, K. N. Matsukage, T. Iguchi, K. Nakayama, and K. Funakoshi (2004), Thermal equation of state of $(Mg_{0.91}Fe_{0.09})_2SiO_4$ ringwoodite, *Phys. Earth Planet. Int.*, *143*, 33–46.
Nishihara, Y., I. Aoki, E. Takahashi, K. N. Matsukage, and K. Funakoshi (2005), Thermal equation of state of majorite with MORB composition, *Phys. Earth Planet. Int.*, *148*, 73–84.
Ohtani, E. (2005), Water in the mantle, *Elements*, *1*, 25–30.
Ohtani, E., T. Shibata, T. Kubo, and T. Kato (1995), Stability of hydrous phases in the transition zone and the upper most part of the lower mantle, *Geophys. Res. Lett.*, *22*, 2553–2556, doi:10.1029/95GL02338.
Ohtani, E., M. Toma, T. Kubo, T. Kondo, and T. Kikegawa (2003), In situ X-ray observation of decomposition of superhydrous phase B at high pressure and temperature, *Geophys. Res. Lett.*, *30*(2), 1029, doi:10.1029/2002GL015549.
Ohtani, E., K. Litasov, T. Hosoya, T. Kubo, and T. Kondo (2004), Water transport into the deep mantle and formation of a hydrous transition zone, *Phys. Earth Planet. Int.*, *143*, 255–269.
Pacalo, R. E. G., and D. J. Weidner (1996), Elasticity of superhydrous B, *Phys. Chem. Miner.*, *23*, 520–525.
Pacalo, R. E. G., and J. B. Parise (1992), Crystal-structure of superhydrous-B, a hydrous magnesium-silicate synthesized at 1400°C and 20 GPa, *Am. Mineral.*, *77*, 681–684.
Palus, S. (2015), Dry minerals in the lower mantle, *Eos Trans. AGU*, *96*, doi:10.1029/5015EO027817.
Peacock, S. M. (1990), Fluid processes in subduction zones, *Science*, *248*, 329–337.
Pearson, D. G., et al. (2014), Hydrous mantle transition zone indicated by ringwoodite included within diamond, *Nature*, *507*, 221–223.
Rosa, A. D., C. Sanchez-Valle, and S. Ghosh (2012), Elasticity of phase D and implication for the degree of hydration of deep subducted slabs, *Geophys. Res. Lett.*, *39*, L06304, doi:10.1029/2012GL050927.
Rosa, A. D., C. Sanchez-Valle, J. Wang, and A. Saikia (2015), Elasticity of superhydrous phase B, seismic anomalies in cold slabs and implications for deep water transport, *Phys. Earth Planet. Int.*, *243*, 30–43.
Schmandt, B., S. D. Jacobsen, T. W. Becker, Z. X. Liu, and K. G. Dueker (2014), Dehydration melting at the top of the lower mantle, *Science*, *344*, 1265–1268.
Schmidt, M. W. (1995), Lawsonite: Upper pressure stability and formation of higher density hydrous phases, *Am. Mineral.*, *80*, 1286–1292.
Shieh, S. R., H. K. Mao, R. J. Hemley, and L. C. Ming (2000), In situ X-ray diffraction studies of dense hydrous magnesium silicates at mantle conditions, *Earth Planet. Sci. Lett.*, *177*, 69–80.
Shukla, G., Z. Q. Wu, H. Hsu, A. Floris, M. Cococcioni, and R. M. Wentzcovitch (2015), Thermoelasticity of Fe^{2+}-bearing bridgmanite, *Geophys. Res. Lett.*, *42*, 1741–1749, doi:10.1002/2014GL062888.
Sinogeikin, S. V., T. Katsura, and J. D. Bass (1998), Sound velocities and elastic properties of Fe-bearing wadsleyite and ringwoodite, *J. Geophys. Res.*, *103*, 20,819–20,825, doi:10.1029/98JB01819.
Sinogeikin, S. V., J. D. Bass, and T. Katsura (2003), Single-crystal elasticity of ringwoodite to high pressures and high temperatures: implications for 520 km seismic discontinuity, *Phys. Earth Planet. Int.*, *136*, 41–66.
Sinogeikin, S. V., J. Z. Zhang, and J. D. Bass (2004), Elasticity of single crystal and polycrystalline $MgSiO_3$ perovskite by Brillouin spectroscopy, *Geophys. Res. Lett.*, *31*, L06620, doi:10.1029/2004GL019559.
Sinogeikin, S. V., J. Bass, D. Lakshtanov, G. Shen, C. Sanchez-Valle, and M. Rivers (2006), Brillouin spectrometer interfaced with synchrotron radiation for simultaneous X-ray density and acoustic velocity measurements, *Rev. Sci. Instr.*, *77*, 103,905.
Speziale, S., and T. S. Duffy (2002), Single-crystal elastic constants of fluorite (CaF_2) to 9.3 GPa, *Phys. Chem. Miner.*, *29*, 465–472.
Stern, R. J. (2002), Subduction zones, *Rev. Geophys.*, *40*(4), 1012, doi:10.1029/2001RG000108.
Suzuki, I. (1975), Thermal expansion of periclase and olivine, and their anharmonic properties, in *Elastic Properties and Equations of State*, edited by T. J. Shankland and J. D. Bass, pp. 145–159, AGU, Washington, D. C.
Tang, Y. C., M. Obayashi, F. L. Niu, S. P. Grand, Y. J. Chen, H. Kawakatsu, S. Tanaka, J. Y. Ning, and J. F. Ni (2014), Changbaishan volcanism in northeast China linked to subduction-induced mantle upwelling, *Nat. Geosci.*, *7*, 470–475.
Thomas, S. M., S. D. Jacobsen, C. R. Bina, P. Reichart, M. Moser, E. H. Hauri, and G. Dollinger (2015), Quantification of water in hydrous ringwoodite, *Front. Earth Sci.*, *2*, 38.
Thompson, A. B. (1992), Water in the Earth's upper mantle, *Nature*, *358*, 295–302.
Ulmer, P., and V. Trommsdorff (1995), Serpentine stability to mantle depths and subduction-related magmatism, *Science*, *268*, 858–861.
Wang, Y. B., D. J. Weidner, R. C. Liebermann, and Y. S. Zhao (1994), P-V-T equation of state of $(Mg,Fe)SiO_3$ perovskite—Constraints on composition of the lower mantle, *Phys. Earth Planet. Int.*, *83*, 13–40.
Watanabe, H. (1987), Physico-chemical properties of olivine and spinel solid solutions in the system Mg_2SiO_4-Fe_2SiO_4, in *High-Pressure Research in Mineral Physics: A Volume in Honor of Syun-iti Akimoto*, edited by M. H. Manghnani and Y. Syono, pp. 275–278, AGU, Washington, D. C.
Zha, C. S., H. K. Mao, and R. J. Hemley (2000), Elasticity of MgO and a primary pressure scale to 55 GPa, *Proc. Natl. Acad. Sci. U.S.A.*, *97*, 13,494–13,499.
Zou, Y. T., S. Greaux, T. Irifune, M. L. Whitaker, T. Shinmei, and Y. Higo (2012), Thermal equation of state of $Mg_3Al_2Si_3O_{12}$ pyrope garnet up to 19 GPa and 1,700 K, *Phys. Chem. Miner.*, *39*, 589–598.